

Independent component analysis of dynamic brain responses during visuomotor adaptation

José L. Contreras-Vidal^{a,b,*} and Scott E. Kerick^a

^aDepartment of Kinesiology, University of Maryland, College Park, MD 20742, USA

^bGraduate Program in Neuroscience and Cognitive Science, University of Maryland, College Park, MD 20742, USA

Received 1 July 2003; revised 29 October 2003; accepted 31 October 2003

To investigate the spatial and temporal changes in electro-cortical brain activity and hand kinematics during the acquisition of an internal model of a novel screen-cursor transformation, we employed single-trial infomax independent component analysis (ICA), spectral estimation, and kinematics methods. Participants performed center-out drawing movements under normal and rotated visual feedback of pen movements displayed on a computer screen. Clustering of task-related and adaptation-related independent components identified a selective recruitment of brain activation/deactivation foci associated with the exposure to the distorted visual feedback, including networks associated with frontal-, central-, and lateral-posterior alpha rhythms, and frontal-central error-related negativity potential associated with transient theta and low beta rhythms locked to movement onset. Moreover, adaptation to the rotated reference frame was associated with a reduction in the imposed directional bias and decreases in movement path length and movement time by late-exposure trials, as well as after-effects after removal of the visual distortion. The underlying spatiotemporal pattern of activations is consistent with recruitment of frontal-parietal, sensory-motor, and anterior cingulate cortical areas during visuomotor adaptation.

© 2004 Elsevier Inc. All rights reserved.

Keywords: Internal model; EEG; Learning; ICA; Functional imaging; Kinematics

Introduction

Pointing movements to visual targets require the transformation of multisensory signals about the spatial target location and hand position into motor commands that move the hand in the direction of the target. This visuomotor transformation must be updated if the visual feedback of movement is distorted by artificially rotating and/or scaling visual space via displacing prisms or computer-based manipulation of cursor-hand relationships. Under such kinematic distortions, practice is needed to acquire an internal

model of the novel environment (Contreras-Vidal and Buch, 2003; Kagerer and Contreras-Vidal, 1997; Krakauer et al., 2000). Thus, visuomotor adaptation requires transformation, integration, modification, and storage of visuospatial and kinesthetic information for movement planning and execution (Buch et al., 2003).

Functional imaging and behavioral studies suggest learning of internal models of distorted kinematic environments involves widespread frontal-parietal interactions (Balslev et al., 2002; Ghilardi et al., 2000; Inoue et al., 2000). Indeed, the superior parietal lobe (SPL) appears to be involved in computing internal spatial representations for target location and hand motion (Lacquaniti et al., 1997; Wolpert et al., 1998) that could be used to compute desired direction of hand movement in visual space (Bullock et al., 1993). Computationally, neuronal populations must estimate, for each limb configuration, an inverse (kinematic) transformation from direction in visual space to direction in motor space. This transformation presumably involves a frontal-parietal network (Burnod et al., 1999; Inoue et al., 2000).

In this study, we combined clustering methods with single-trial infomax independent component analysis (infomax ICA; Makeig et al., 2002), time-frequency analysis techniques of high-density EEG data, and detailed kinematic analysis of movement trajectories during exposure to a rotational distortion. The aims were to uncover the recruitment of task-specific and adaptation-specific compact cortical domains and rhythms across different stages of learning.

Methods

Participants

Ten healthy right-handed adults (mean age 27.8 ± 7.2) volunteered to participate in the study after giving informed consent. All subjects had normal or corrected-to-normal vision. All procedures were approved by the Institutional Review Board at the University of Maryland-College Park.

Apparatus

Subjects sat at a table facing a flat computer screen (14 display at eye level) that was situated in front of them at a distance of

* Corresponding author. Department of Kinesiology, University of Maryland, 2363 HHP Building, College Park, MD 20742. Fax: +1-301-405-5578.

E-mail address: pepeum@umd.edu (J.L. Contreras-Vidal).

Available online on ScienceDirect (www.sciencedirect.com.)

approximately 60 cm and performed “center-out” drawing movements on a digitizing tablet (12 WACOM InTuos), which was placed lateral to the subject’s midline. The subjects’ task was to draw lines from a red circle in the center of the screen to one of four blue target circles (all diameters = 5 mm, each at 10 cm from the origin and located at 45° , 135° , 225° , and 315°) on the display. Pen trajectories were sampled at 200 Hz using custom *Oasis v.8.29* software (*Kikosoft*, Neijmegen.) and displayed in real time on the computer screen, with movement paths depicted as solid black lines. A vertical board prevented vision of the arm/hand. Electrophysiological signals were recorded by using an Electro-cap with 64 tin electrodes placed according to the extended International 10-20 system while subjects performed the task inside an $8' \times 10'$ shielded room. Electrode sites with impedances higher than 10 k Ω were rejected, resulting in 46 ± 7 (mean \pm 1 SD) electrode sites used for further analysis. Continuous EEG signals were sampled at 500 Hz, amplified ($\times 500$), and digitally filtered (0–100 Hz) via a Synamps acquisition system and Neuroscan v.4.1 software. A linked-ears reference was employed with FPz as ground. Electro-ocular activity was measured with a bipolar electrode montage with electrodes attached superior and inferior to orbital fossa of the right eye for vertical eye movement (veog) and to the external canthi for horizontal eye movement (heog). Amplifiers were calibrated for each participant separately through source input of a 50- μ V, 10-Hz sinusoidal wave at all channels simultaneously. Event markers generated by custom OASIS software synchronized start of trial, movement onset, target appearance and acquisition time, and trial abortion time with the EEG signals. The participant’s head was stabilized to minimize muscle artifact using a chin rest and nose bridge head positioner (*QuickClamp*, Arrington Research Inc.).

Experimental procedure

The experimental session consisted of 240 trials, including 20 practice trials administered at the beginning of the session to familiarize the subjects with the experimental setup. These practice trials were not analyzed further. Thus, trials 21–40 (preexposure condition) were performed under normal visual feedback of cursor movement (e.g., the direction and size of the pen movement performed on the digitizing tablet were in 1:1 relationship with the screen cursor movement displayed on the computer display). Trials 41–220 (exposure condition) were performed under a screen cursor rotation of 60° counterclockwise, whereas trials 221–240 (postexposure condition) were performed under normal visual feedback to test for after-effects.

Movements were self-initiated and all targets were displayed throughout each trial. Entering the home target started a trial. The

task instructions were to position the screen cursor linked to the pen inside the red target, to select one of the four blue targets while keeping the pen still inside the home circle, and ‘when ready,’ to draw a line between the red and the chosen blue target ‘as fast and as straight as possible.’ Moreover, subjects were instructed to avoid any patterning in the selection of the blue targets (e.g., clockwise target sequencing). Unknown to the participants, trials for which elapsed movement time between entering the home target and starting a red-to-blue targeted movement was less than 2 s were aborted and the trial was restarted (Fig. 1). This provided participants with ample target selection and movement planning time and provided an extended window to study cortical activations associated with planning and preparation processes. After a successful trial (e.g., upon the subject entering the blue target circle), all visual stimuli were erased from the screen in preparation for the next trial. Inter-trial intervals were variable (in fact, self-paced by the subject), but at least with a duration of 2 s. Brief rest periods were allowed as needed to minimize fatigue and maintain attention.

Data analysis

Movement kinematics

The sampled Cartesian position data were low-pass filtered using a 5-Hz, dual-pass eighth-order Butterworth filter. A vector from the home target to the pen position at 80 ms after movement onset determined the initial direction of the planned movement trajectory. The initial directional error (IDE) was calculated as the angular difference between this vector and a vector extending from the home position to the target. IDE is thought to represent early visuomotor transformations for movement, and thus, the current state of the internal model of the distorted environment (Buch et al., 2003). Movement time (MT) was defined as the time elapsed between leaving the home target and acquiring the blue target, whereas movement length was defined as the length of the trajectory from the home to the target position. Nonparametric statistical analysis of the kinematic data using the Wilcoxon signed ranks test was used to assess initial response (early exposure) to the distorted environment, final adaptation levels (late exposure), and after-effects (postexposure).

Signal processing

Continuous EEG data were epoched in 3-s windows around the movement onset trigger from 2 s preceding (-2 s) to 1 s following ($+1$ s) movement onset. Single-trial data were detrended to remove DC amplifier drift, low-pass filtered below 40 Hz to suppress line noise, and baseline-corrected by averaging the mean potential from -2 to 1 s.

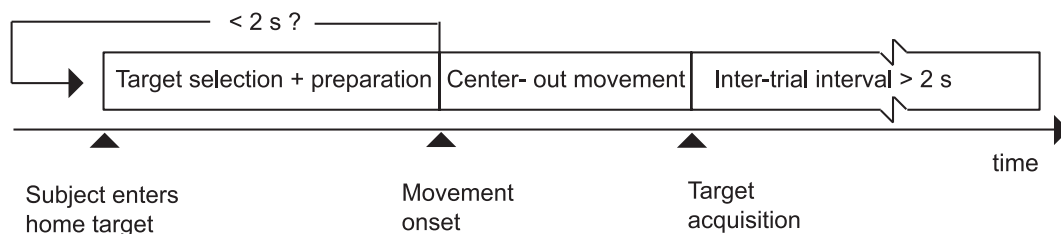


Fig. 1. The experimental time for each trial. Each trial starts when the participant enters the home (central) target, at which time he or she selects a peripheral target and prepares the movement. Unknown to the participant, target selection and preparation times of less than 2 s result in an aborted trial, which can be restarted by entering the home target again. In a successful trial, a center-out movement leads to acquisition of the desired peripheral target. Inter-trial intervals are self-paced by the participant, but of at least 2 s in duration.

Independent component analysis and clustering

Infomax independent component analysis (ICA) (Makeig et al., 2002; MatLab toolbox available at <http://www.sccn.ucsd.edu>) was applied in a *single-trial* basis to derive spatial filters by blindly separating the input data into a sum of temporally independent and spatially fixed components arising from distinct or overlapping brain or extra-brain sources (e.g., 60 Hz line noise). These spatial filters were used to evaluate changes in task-related and adaptation-related electro-cortical activity as subjects were exposed to the new visuomotor environment. The application of ICA to EEG data makes the following reasonable assumptions: the existence of statistically independent amplitude distributions of the source signals, their instantaneous linear mixing at the scalp sensors, and the stationarity of both the source signals and the mixing process (see Vigarío et al., 2000, for discussion of the validity of applying ICA to EEG data).

Single-trial ICA activations in the -2 to $+1$ s (aligned to movement onset) were first clustered and analyzed within blocks of 20 consecutive trials from preexposure to postexposure trials resulting in 11 blocks. Before ICA clustering, the ICA-processed EEG data were visually inspected for eye, muscle, and non-brain artifacts as described in Jung et al. (2000, 2001). As the number of accepted electrode sites varied across subjects, thin-plate smoothing splines (MatLab *tpaps* method) were used to interpolate the ICA scalp maps. Component clustering was performed in two consecutive steps. Step 1: the K-means clustering algorithm (MatLab *kmeans* method) was used to partition the *single-trial* component maps across subjects and within each block into K mutually exclusive clusters by minimizing the sum of squared Euclidian distances from each object to its cluster centroid (e.g., the mean of the points in that cluster) over all clusters. K-means finds a partition in which the actual observations within each cluster are as close to each other as possible, and as far from objects in other clusters as possible. Step 2: the resulting K-means centroids from Step 1 were further clustered across blocks using the hierarchical clustering method based on the Euclidean distance, where clusters at one level are joined as clusters at the next higher level. The average distance between all pairs of objects (i.e., centroids from Step 1) comprising any of two groups was used to generate the hierarchical cluster tree information. The cophenetic correlation coefficient, which measures the distortion of the classification, was computed to assess the quality of the structure suggested by the classification (MatLab *cophenet* command). The two-step clustering algorithm did not use a priori information about the number of task and adaptation-related clusters, their topography, or the subject's identity. In principle, the clustering algorithms can discriminate or pull out ICA clusters from individual subjects if their ICA components were different across the experiment. Thus, ICA clusters found across subjects represent consistent task and adaptation-related network activations across the population.

Power spectral density (PSD) of the cluster-mean activations was computed using the Thomson multi-taper method (*pmtm* Matlab command). This method uses nonlinear combinations of modified periodograms to estimate the PSD. These periodograms are computed using a sequence of orthogonal tapers (windows in the frequency domain) specified from the discrete prolate-spheroidal sequences. Time-frequency representations used the Kaiser's approximation to the prolate-spheroidal windows ($\beta = 5$, relative side lobe attenuation = -36.9 dB) moved through the 3-s data epochs (from -2 s before to 1 s after movement onset) in 2-ms steps.

Event-related potentials

Response-locked event-related potential (ERPs) were quantified by measuring area, peak amplitude, and slope of the electrical activity at the central midline (CZ) and lateral–frontal (FC1) electrodes after ICA-based removal of eye, muscle, and non-brain artifacts as described in Jung et al. (2000). Three time windows were used: -1.5 to -0.5 s, -0.5 to 0 s, and 0 to 0.5 s with respect to movement onset ($t = 0$ s). These ERP measures at the early- and late-exposure adaptation stages were entered into a MANOVA to analyze the effects of exposure to the screen cursor rotation on error- and adaptation-related ERPs.

Results

We observed a complex pattern of changes in both planning and control aspects of hand kinematics, and in the electro-cortical potentials as subjects adapted to the rotated visual feedback. Fig. 2A depicts pen trajectories during pre-, early-, middle-, late-, and postexposure trials. In preexposure trials, subjects performed straight movements to the target; however, in early exposure, the sudden introduction of the rotational distortion resulted in movement trajectories that resembled mostly counterclock spirals, with sudden reversals, jagged trajectories, and slow progression (Roby-Brami and Burnod, 1995). Nevertheless, by late-exposure trials movement trajectories were straighter and smoother (although some spirals remained). After removal of the distortion, movement trajectories showed distortions (after-effects) in the opposite direction as during exposure.

Changes in movement control were indexed by time spent during the center-out movement (MT), and by the movement length (ML) traveled in each trial (Fig. 2B). Changes in movement planning were indexed by the initial directional error (IDE). Significant increases in movement time (block means: pre = 0.75 ± 0.34 ; early = 2.52 ± 1.27 s), movement length (block means: pre = 11.72 ± 1.24 ; early = 19.32 ± 4.16 cm), and initial directional errors (block means: pre = -6.2 ± 6.39 ; early = $-53.36 \pm 29.5^\circ$) were found immediately after the introduction of the visual distortion in early exposure (all Wilcoxon tests: $P < 0.01$). As expected, a rapid improvement in MT (block means: late = 1.24 ± 0.55 ; early = 2.52 ± 1.27 s) and ML (block means: late = 13.91 ± 2.72 ; early = 19.32 ± 4.16 cm), and a gradual improvement in IDE (block means: late = -49.07 ± 34.02 ; early = $-53.36 \pm 29.5^\circ$) were observed with practice by late exposure (all Wilcoxon tests: $P < 0.05$). As illustrated by the distorted movement trajectories at postexposure (in the absence of visual distortion; see Fig. 2A), there were significant ($P < 0.05$) after-effects for MT (block means: post = 0.96 ± 0.4 ; pre = 0.75 ± 0.34 s) and ML (block means: post = 13.31 ± 2.77 ; pre = 11.72 ± 1.24 cm), with the IDE after-effect almost reaching significance ($P = 0.074$). Thus, by late exposure, participants have acquired, at least partially, the internal model of the visuomotor transformation.

Clustering of the single-trial infomax ICA-decomposed independent components across subjects and exposure blocks (totaling 100,240 components) resulted in consistent cluster-means (cophenetic correlation: $c = 0.7902$). Each cluster-mean was characterized by a different, fixed scalp map representing the spatial projection of the component to each scalp site, a time course of activation, and power spectral density (Figs. 3, 5, and 6). Fig. 3 shows an ICA cluster with a fixed frontal–central (FC) scalp projection that had a strong negativity at approximately 80 ms after movement onset (Fig. 3B). This cluster appeared in all phases of adaptation (from

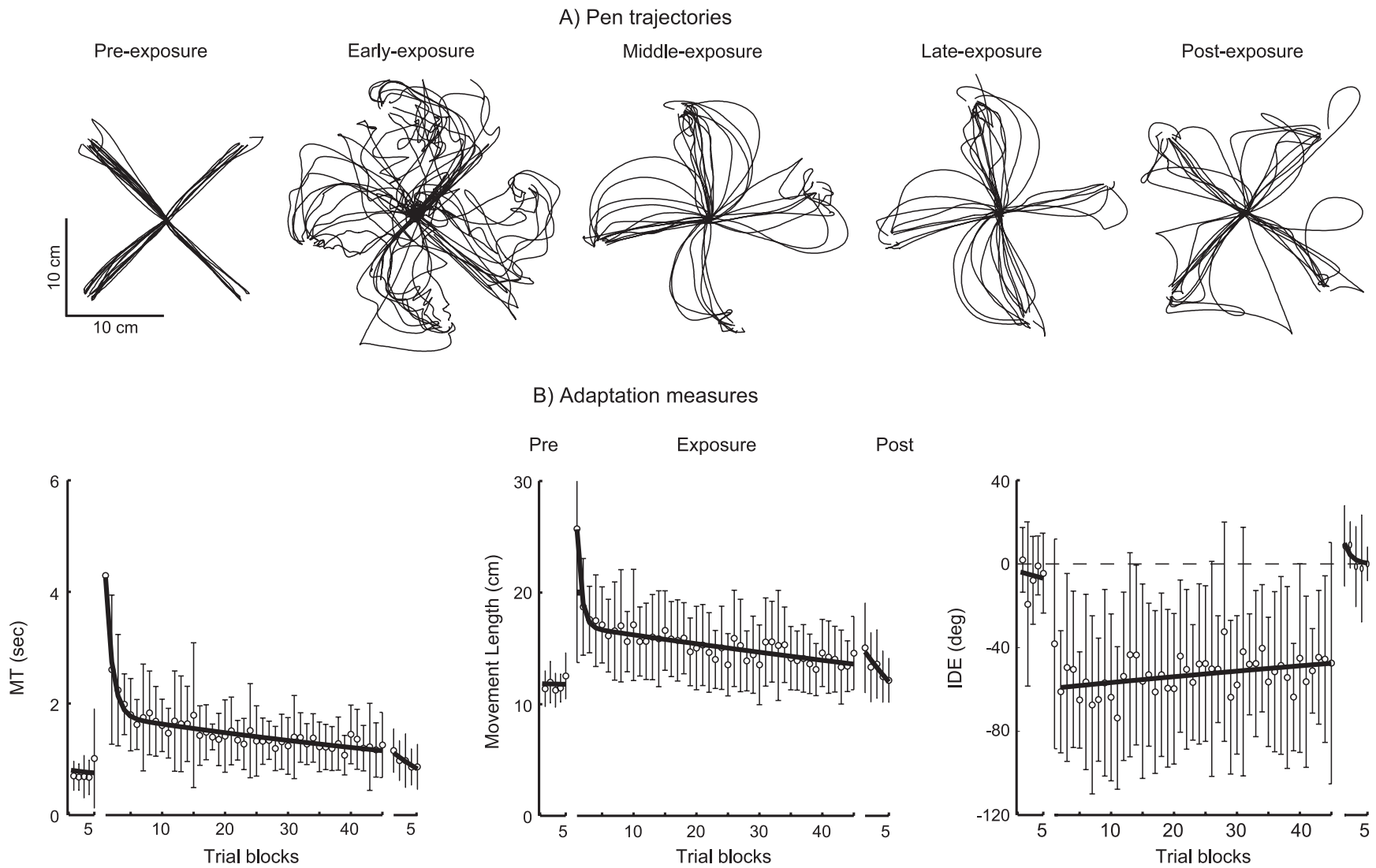


Fig. 2. (A) Pen trajectories during pre-, early-, middle-, late-, and postexposure trials. (B) Adaptation measures for movement time (MT), movement length (ML), and initial directional error (IDE) as a function of trial block (mean \pm SD) of four consecutive trials. Bold lines represent best fits based on the Nelder–Mead Simplex algorithm (Buch et al., 2003). The preexposure (linear fit), exposure (double exponential fit), and postexposure (single exponential fit) conditions have been fitted separately.

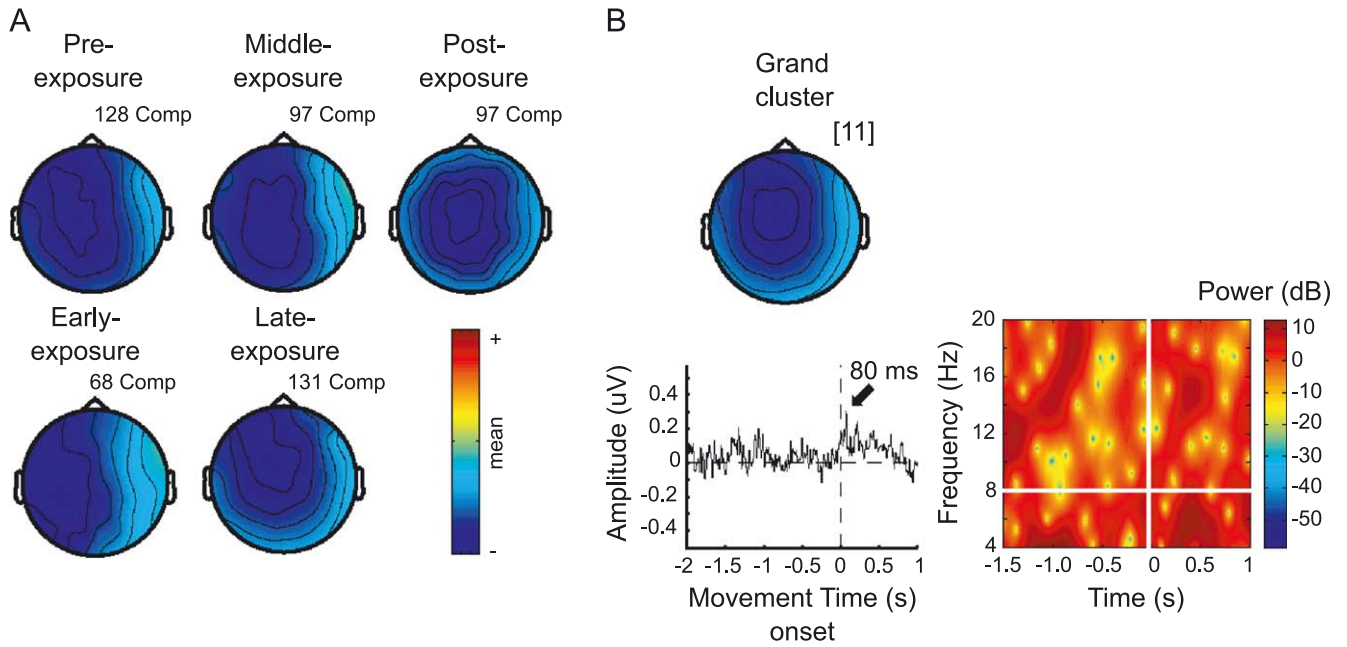


Fig. 3. (A) Cluster-mean independent components for error-related negativity (ERN) generated across pre-, early-, middle-, late-, and postexposure blocks (see Methods). (B) Grand cluster and its mean component activation and time-frequency representation for time -1.5 s to $+1$ s. At time $t = 0$ s, the movement onset is represented. Note the transient increase in theta and low beta rhythms after movement onset. Grand cluster represents the average of cluster-means in pre-, early-, middle-, late-, and postexposures as found by the hierarchical clustering algorithm.

preexposure to postexposure blocks) and its time-frequency representation showed a transient increase in theta (4–8 Hz) and low beta (12–18 Hz) rhythms locked to movement onset. The transient increase in beta power appears to peak around 250–350 ms after onset. Pfurtscheller et al. (1997) showed post-movement beta synchronization within the first second after movement onset in participants performing self-paced finger movements. This effect was interpreted as active inhibition following movement execution.

Such an interpretation is consistent with the present findings in that movement toward the target would need to be inhibited as the pen (a) approached its target destination and/or (b) needed to be redirected in response to the distortion of visual feedback.

The effects of exposure on error-related and adaptation-related ERPs were also quantified by measuring the area, peak amplitude, and slope in the response-locked ERPs at the central midline (Cz) and lateral–frontal (FC1) electrodes in the -1.5 to -0.5 s, -0.5 to

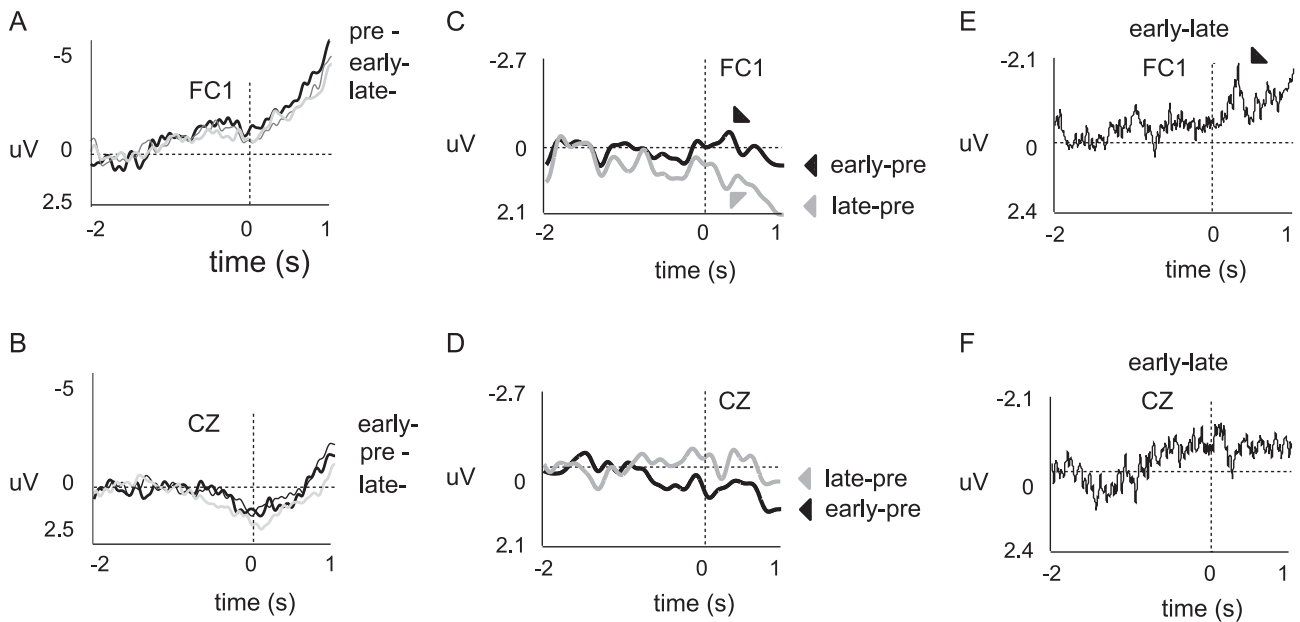


Fig. 4. Event-related potentials (ERPs) as a function of adaptation stage to rotated visual feedback of movement. Slow cortical potentials (A, B), subtraction waveforms (early–preexposure and late–preexposure trials: C, D), and subtraction waveforms (early–late-exposure: E, F) for the FC1 and CZ electrodes are shown. Response onset occurs at time = 0 s. Relevant waveform peaks, marked by the arrows, occur approximately at 250 ms after movement onset.

0 s, and 0 to 0.5 s time windows (Figs. 4A, B). A significant effect of adaptation stage [$F(3,7) = 0.331, P < 0.05$] for CZ was found (Fig. 4B). The area under the curve was reduced from early (114 μV^2) to late exposure ($-41 \mu\text{V}^2$) [$F(1,9) = 7.448; P < 0.05$], and the peak amplitude in late-exposure trials ($-2.02 \mu\text{V}$) was less positive than in early-exposure trials ($-1.25 \mu\text{V}$) [$F(1,9) = 16.326; P < 0.005$]. With respect to the FC1 scalp site, the effect of adaptation stage almost reached significance [$F(3,7) = 0.36, P = 0.055$]. In this case, the slope of the negative-going potential in the early-exposure trials ($-1.6 \mu\text{V/s}$) was less positive than in the late-exposure trials ($-0.056 \mu\text{V/s}$) [$F(1,9) = 3.348; P < 0.097$]. To further quantify the exposure-related changes, subtraction waveforms (early–preexposure and late–preexposure trials) were obtained at the lateral–frontal (FC1) and central midline (CZ) electrodes. A 10-Hz low-pass digital filter was applied to the response-locked ERP averages (Figs. 4C, D). With respect to the lateral–frontal site, the waveforms for the preexposure (low visuomotor error trials) and early exposure (high visuomotor

error trials) cancelled each other out, whereas the late–preexposure subtraction resulted in a slow positive waveform (Fig. 4C). The opposite pattern was observed when comparing the subtraction waveforms at the central midline electrode (Fig. 4D). In this case, the early–preexposure comparison showed an increasing positivity, whereas the late–preexposure subtraction nullified the resulting waveform. The effects of the distorted visual feedback on the FC1 and CZ potentials can be seen clearly in the early–late-exposure subtraction waveforms (Figs. 4E, F). Specifically, a prominent negativity peak at 250 ms with respect to movement onset can be seen at the lateral–frontal scalp site.

Fig. 5A shows a lateral–posterior (LP) cluster with upper alpha (10–12 Hz) and less prominent theta (4–8 Hz) spectral content. This cluster was not seen during postexposure trials. In addition, a nearby negativity localized in the central–posterior (CP1) region with less prominent alpha activity was also found (Fig. 5B). A third ICA cluster in the central–medial (CM, Fig.

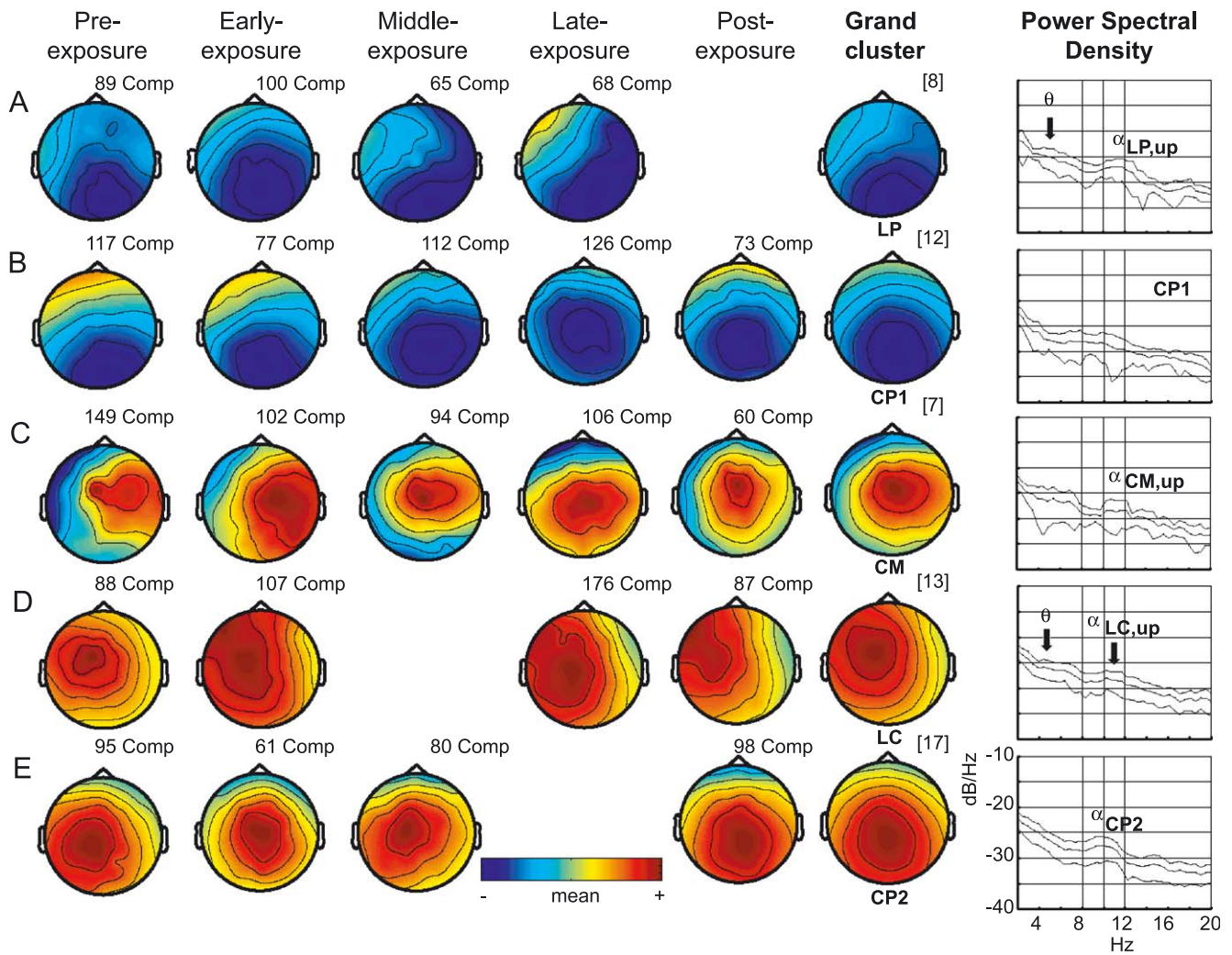


Fig. 5. (A–E) Mean component activations (depicted as mean scalp maps) and power spectral densities (PSD, mean \pm 1 SD) for the grand clusters of independent components observed across all exposure stages. These five grand clusters identify a task-related visuomotor network for hand movements to visual targets. Each of these grand clusters comprised 7–17 cluster-mean independent components across pre-, early-, middle-, late-, and postexposure blocks (see Methods). Keys: FC, frontal central; CP, central posterior; LC, lateral central; CM, central medial; LP, lateral posterior; $\alpha_{\text{CM, up}}$, central medial upper (10–12 Hz) alpha; α_{CP} , central posterior (8–12 Hz) alpha; $\alpha_{\text{FC, up}}$, frontal central upper alpha; θ , theta (4–8 Hz) band.

5C) scalp region showed strong spectral content in the upper (10–12 Hz) alpha band, and time-frequency analysis showed transient theta activity locked to movement onset (not shown). This cluster had the lowest number of components ($N = 7$) as it was not seen in 4 of the 11 blocks. Interestingly, the peak activation for this CM cluster was highly focused during pre-exposure, but expanded during the early-exposure block. However, by the middle- and late-exposure blocks, the spread of activation had been reduced. A fourth lateral–central (LC, Fig. 5D) cluster also showed an expansion during exposure blocks that was not reduced with practice. Time-frequency analysis showed that this cluster produced a modest theta activity locked to movement onset and upper alpha activity during the pre-movement period. A fifth cluster with strong 10-Hz alpha power in the central–posterior (CP2) area was also found (Fig. 5E). Time-frequency analysis showed that this alpha rhythm was concentrated around movement onset.

Fig. 6 shows ICA clusters that emerged during exposure to the distortion, but not during preexposure trials. One grand cluster, comprising five mean ICA component activations, had a lateral (left)–posterior scalp topography that appeared during middle- and late-exposure trials only (cluster LP_d in Fig. 6F). Its activation consisted of low theta (4–6 Hz) and broad alpha (8–12 Hz) rhythms. A second cluster had a central–posterior activation which appeared during early- and middle-exposure trials, but not during late exposure (grand cluster labeled CP1_d). Its spectral content was unremarkable (Fig. 6G). The third cluster was localized in the lateral (right)–central scalp sites and showed oscillatory activity in the low (8–10 Hz) alpha and beta (16–20 Hz) bands (grand cluster labeled LC_d in Fig. 6H). This cluster was seen in all stages of adaptation after preexposure. A central–posterior (CP2_d) cluster, with a broad alpha content and transient theta activity locked to movement onset, was also seen across all exposure and postexposure trials (Fig.

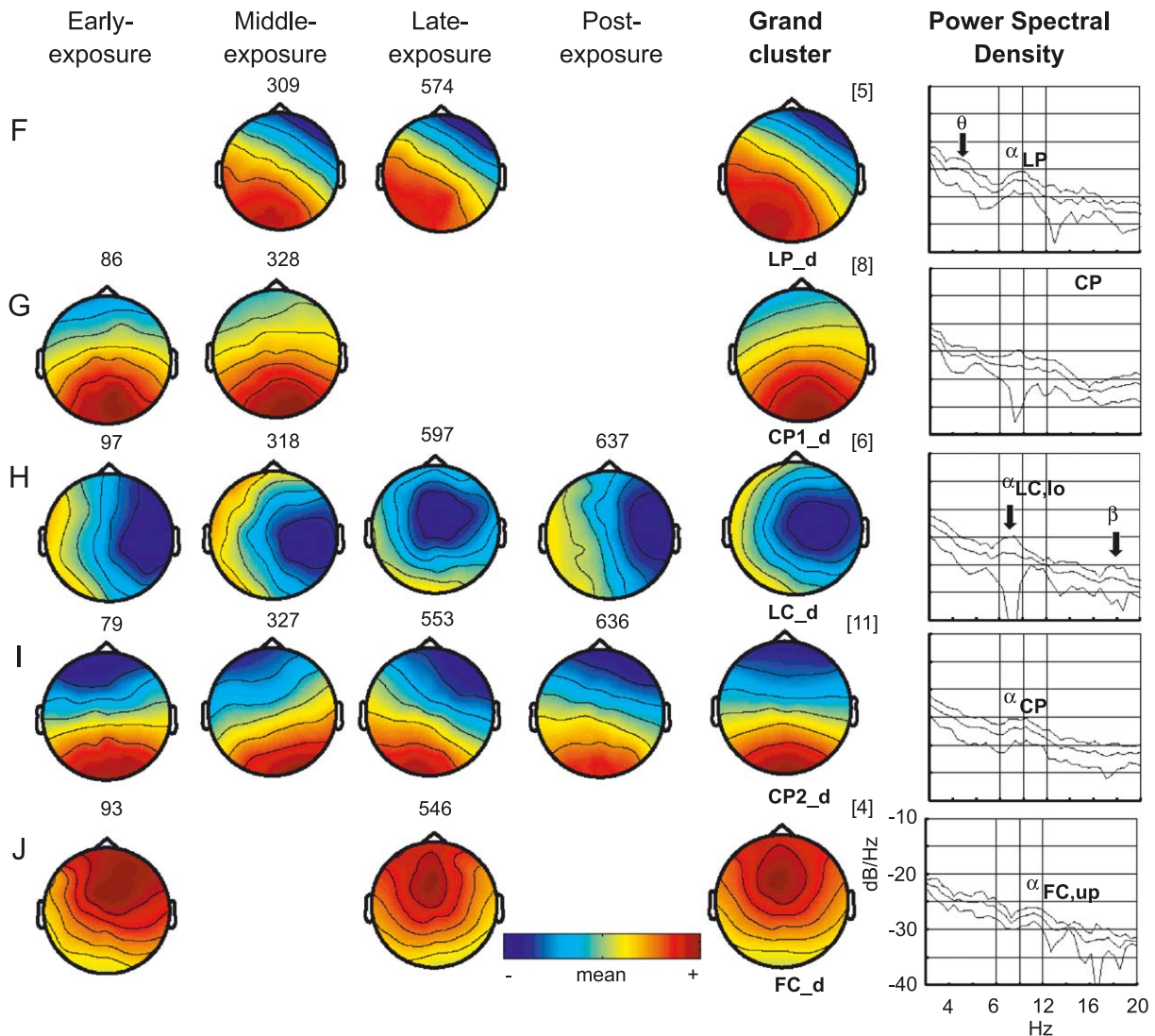


Fig. 6. (F–J) Mean component activations (depicted as mean scalp maps) and PSD for grand clusters of independent components observed during exposure and postexposure blocks (but not during preexposure trials) and recruited in addition to the basic frontoparietal network seen in Figs. 2 and 3. Each of these grand clusters comprised 4–11 cluster-mean independent components across early-, middle-, late-, or postexposure blocks (see Methods). See Fig. 5 for the key abbreviations. Subindex ‘d’ denotes clusters seen during distorted trials only.

6I). A fifth cluster with frontal–central (LC_d) activation showed upper alpha and some pre-movement theta activities (Fig. 6J). It was seen only during early and late-exposure trials.

Discussion

Clustering of single-trial independent components blindly separated by infomax ICA revealed a consistent parietal–frontal network for hand movements to visual targets with similar scalp distributions across pre-, early-, middle-, late-, and postexposure conditions. Interestingly, this basic visuomotor network was expanded to include additional central– and lateral–posterior, lateral–central, and frontal–central scalp sites when subjects were exposed to the distorted environment. The significance of these activation patterns is discussed next based on a hypothesized adaptive frontoparietal network that performs visuomotor transformations for reaching (Fig. 7).

In this scenario, visual and/or proprioceptive signals about target location and end-effector position are used to code internal representations for ‘target’ and ‘arm’ in visuospatial coordinates, presumably in posterior parietal cortex (PPC). These internal representations can be vectorially compared to compute a spatial difference vector (DVs). There is growing experimental evidence that the visuomotor transformation from direction in

visual space (DVs) to direction in (pre)motor space (DVm) involves a parieto-premotor network that includes rostral and caudal premotor areas, superior and inferior parietal areas, and the intraparietal sulcus (Burnod et al., 1999; Inoue et al., 2000). This spatial direction-to-joint rotation (visuomotor) transformation is an inverse kinematic transformation and computationally, it can be learned through certain amount of simultaneous exposure to patterned proprioceptive and visual stimulation under conditions of self-produced movement—called “motor babbling” (Bullock et al., 1993). In the model, the anterior cingulate cortex (ACG) performs action monitoring to detect unexpected performance errors (Carter et al., 1998; Falkenstein et al., 2001). Thus, whenever a visuomotor discrepancy is detected (e.g., due to manipulation of cursor–hand relationships as in the present study), it is hypothesized that the ACG activation would lead to recruitment of additional frontoparietal structures for updating of the visuomotor network.

Error-related negativity cluster

A consistent frontal–central cluster, whose negativity peaked approximately at 80 ms after movement onset, was found across all 11 blocks from pre- to postexposure. An event-related potential (ERP) with similar scalp topography and timing, called error negativity (ERN), is generated when subjects make errors in

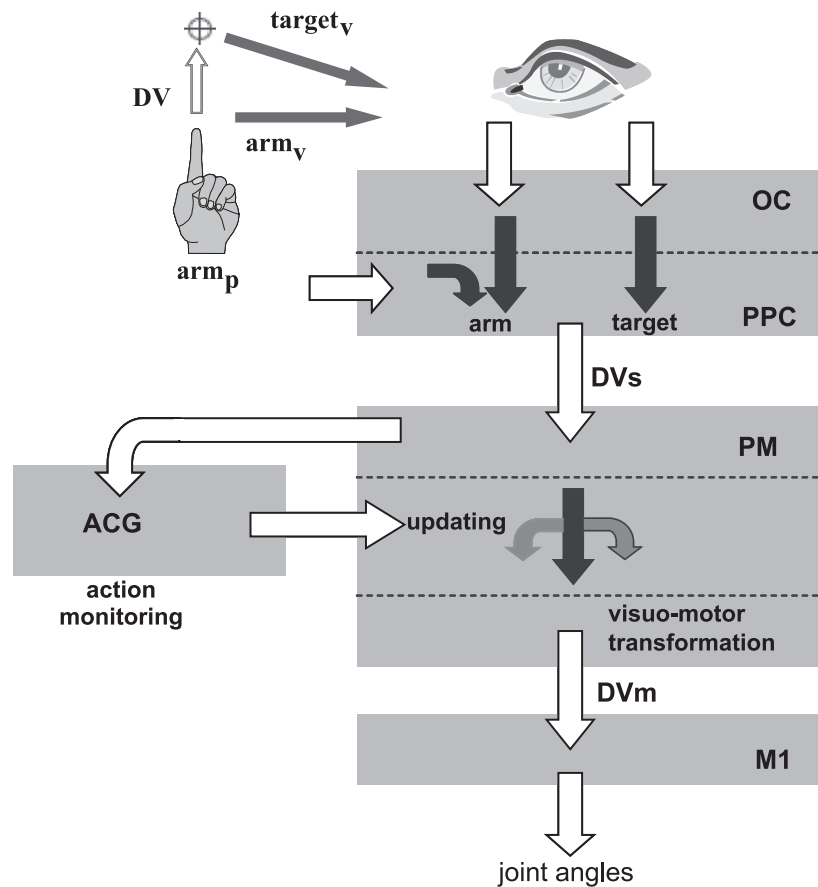


Fig. 7. Hypothetical adaptive frontoparietal network for visuomotor transformations for reaching. Keys: ACG, anterior cingulate cortex; OC, occipital cortex; PPC, posterior parietal cortex; PM, premotor cortex; M1; primary motor area; DVs, spatial difference vector; DVm; joint rotations; arm_p, proprioceptive information about end-effector position; arm_v, visual information about end-effector position; target_v, visual information about target location.

reaction time tasks. It has been associated with error monitoring and on-line error correction (Falkenstein et al., 2001; Rodríguez-Fornells et al., 2002; Swick and Turken, 2002), response competition (Carter et al., 1998), and conflict monitoring (Swick and Turken, 2002). The ERN, which it is thought to originate in the anterior cingulate cortex (ACC), is present not only during erroneous motor responses, but also during correct responses (Carter et al., 1998). In the present study, a consistent cluster with a frontal–central negativity was present in both undistorted (with low visuomotor errors) and distorted trials (with high visuomotor errors) early after movement onset. This is consistent with the mean and standard deviation of the initial directional error (IDE) scores in the present experiment. Specifically, the mean preexposure IDE shows that the initial movement direction was slightly biased in the direction of the distortion, whereas the IDE standard deviation shows that small directional errors occurred during preexposure trials (e.g., second trial block in IDE score of Fig. 2B). Thus, error-related negativity would also be expected in preexposure trials. Importantly, assessment of the directional error 80 ms after movement onset allows the error to be measured before corrections guided by visual feedback are employed. Thus, the IDE represents a behavioral measure of the planned initial movement direction, and hence a measure of acquisition of the ‘internal model’ of the novel environment.

It has been proposed that the performance-monitoring functions reflected in the time course of the ERN may involve the comparison of the intended response with the predicted response, estimated from the output of an internal (forward) model activated by an efference copy of the motor command (Rodríguez-Fornells et al., 2002; Swick and Turken, 2002). Thus, the frontal–central negativity observed in the present study may be related to performance monitoring to detect errors required to adapt the internal visuomotor representation to the rotated environment. Moreover, the present findings suggest that an ERN-like activity is also generated during volitional, self-initiated movement tasks. Interestingly, the transient post-movement onset theta activity found in this frontal–central cluster is also consistent with EEG/MEG reports of a source for theta rhythms in the anterior cingulate and medial prefrontal cortex during updating, maintenance, and recall of working memory representations (Asada et al., 1999; Gevins et al., 1997; Iramina et al., 1996).

An analysis of subtraction waveforms resulted in opposite patterns at lateral–frontal and central midline electrode sites. In particular, compared to preexposure trials, visuomotor errors during early-exposure (early–pre) trials resulted in a less negative potential at the central midline (CZ) electrode site, which was reestablished by late-exposure trials. This may suggest that after extended practice in the distorted environment, movement planning/preparation processes were again functional. Conversely, at the lateral–frontal site, slow negative potentials during early and preexposure trials were similar, and they were reduced by late exposure. Subtraction waveforms at this site showed peaks of opposite polarity at approximately 250 ms post-movement onset, with the early–preexposure comparison showing a phasic increase in negativity due to high errors in this early-exposure condition. Comparison of early–late waveforms confirmed this peak negativity at 250 ms post-movement onset.

Results from the ICA clustering showed an error-related negativity cluster that peaked approximately at 80 ms after movement onset, while the subtracted waveforms of error-related ERPs peaked at 250 ms after movement onset. Although it may be

tempting to compare the ICA-clustered activation with the subtracted response-locked ERP waveforms, this may not be appropriate as the latter represent a mixture of sources at the underlying scalp site(s), while the ICA-found negativity represents a unique, temporally independent (from other clusters of cortical activations), spatially fixed cluster of sources. It is likely that the time gap (80 ms versus 250 ms) may result from the mixture of many task-related sources that shape the ERP potentials at the scalp sites. Thus, ICA may provide better time resolution and waveform discrimination than traditional averaging methods.

Occipital–parietal deactivation cluster (CP1)

This cluster had a maximum of deactivation in visuoparietal areas that may be related to attentive visual movement control (Seitz et al., 1997) and/or the internal representation for visual target location (Kawashima et al., 1995). This cluster was observed in all blocks, and appeared to expand to central anterior sites during middle- and late-exposure blocks before contracting in postexposure to the same level as in preexposure.

Posterior parietal activation cluster (CP2)

This cluster localized to the central posterior scalp region showed a strong spectral peak in the alpha band. Its activation showed some spatial overlap with the visuoparietal negativity. Moreover, it showed an increase in activation that appeared to be locked to movement onset, not unlike that seen in the frontal–central error-related negativity reviewed above. The alpha activity in this cluster may reflect internal mental activity rather than an idle state (Von Stein and Sarnthein, 2000), such as that related to visuomotor transformations for arm movement.

Lateral and medial premotor activation clusters (CM and LC)

Maximal upper alpha power localized to the central–medial scalp sites was observed in 7 of the 11 blocks (grand cluster CM in Fig. 5). The scalp projection of this activation was highly focalized, except at early-exposure trials, where it extended to posterior and lateral sites in the right hemisphere. A second activation localized to the central lateral sites in the left hemisphere was also observed (grand cluster LC in Fig. 5). This activation had components in the theta and upper alpha bands, and it expanded from pre- to early exposure, which may suggest increased top–down internal processing related to changes in visuomotor transformations during early exposure.

Left and central occipital activation clusters (CP1_d, CP2_d, and LP_d)

A cluster localized to the central occipital scalp sites was observed in early- and middle-exposure blocks only (grand cluster CP1_d in Fig. 6). However, by middle- and late-exposure blocks, an additional activation that shifted laterally to the left hemisphere was observed, which was accompanied by prominent increases in both theta and alpha power (grand cluster LP_d in Fig. 6). A third cluster, which appeared in early-, middle-, late-, and postexposure blocks, also had a strong alpha component (CP2_d). Its activity projected in the central occipital area and decreased from early to postexposure trials. These activations may be related to the updating of internal

target/cursor representations and/or whole-field visual representations (Seitz et al., 1997). Moreover, this set of visuoparietal clusters may be related to the spiral-like cursor trajectories seen during the rotated trials.

Right sensorimotor deactivation cluster (LC_d)

This cluster had components in the low alpha (8–10 Hz) and beta (16–18 Hz) bands, which projected to the scalp as a focal negativity in the ipsilateral hemisphere. The biological significance of this cluster is not clear.

Frontal activation cluster (FC_d)

A compact cluster of frontal central activation had upper alpha power specific to early- and late-exposure trials, with the spread of activation slightly larger at early exposure. It may represent activation related to selection of corrective actions during exposure in response to internal mismatches between intended and actual responses (e.g., ERN).

In summary, adaptation to the rotated reference frame was associated with a reduction in the imposed directional bias, and decreases in movement length and movement time by late-exposure trials, as well as after-effects after removal of the visual distortion. These kinematic changes were associated with spatio-temporal pattern of activations consistent with recruitment of frontal–parietal areas concerned with visuomotor transformations for hand movement and frontal–central areas, presumably anterior cingulate and medial prefrontal cortices related to performance monitoring, error detection, and response selection required to adapt the internal visuomotor representation for movement.

Acknowledgments

This work was supported by NIA Grant AG19148. The authors wish to thank Brad Hatfield for useful discussions.

References

- Asada, H., Fukuda, Y., Tsunoda, S., Yamaguchi, M., Tonoike, M., 1999. Frontal midline theta rhythms reflect alternative activation of prefrontal cortex and anterior cingulate cortex in humans. *J. Cogn. Neurosci.* 14, 70–78.
- Balslev, D., Nielsen, F.Å., Frutiger, S.A., Sidtis, J.J., Christiansen, T.B., Svarer, C., Strother, S.C., Rottenberg, D.A., Hansen, L.K., Paulson, O.B., Law, I., 2002. Cluster analysis of activity-time series in motor learning. *Hum. Brain Mapp.* 15, 135–145.
- Buch, E.R., Young, S., Contreras-Vidal, J.L., 2003. Visuomotor adaptation in normal aging. *Learn. Mem.* 10, 55–63.
- Bullock, D., Grossberg, S., Guenther, F.H., 1993. A self-organizing neural model of motor equivalent reaching and tool use by a multijoint arm. *J. Cogn. Neurosci.* 5, 408–435.
- Burnod, Y., Baraduc, P., Battaglia-Mayer, A., Guigon, E., Koechlin, E., Ferraina, S., Lacquaniti, F., Caminiti, R., 1999. Parieto-frontal coding of reaching: an integrated framework. *Exp. Brain Res.* 129, 325–346.
- Carter, C.S., Braver, T.S., Barch, D.M., Botvinick, M.M., Noll, D., Cohen, J.D., 1998. Anterior cingulate cortex, error detection, and the online monitoring of performance. *Science* 280, 747–749.
- Contreras-Vidal, J.L., Buch, E.R., 2003. Effects of Parkinson's disease on visuomotor adaptation. *Exp. Brain Res.* 150, 25–32.
- Falkenstein, M., Hoormann, J., Hohnsbein, J., 2001. Changes of error-related ERPs with age. *Exp. Brain Res.* 138, 258–262.
- Gevins, A., Smith, M.E., McEnvoy, L., Yu, D., 1997. High-resolution EEG mapping of cortical activation related to working memory: effects of task difficulty, type of processing, and practice. *Cereb. Cortex* 7, 374–385.
- Ghilardi, M.F., Ghez, C.V., Dhawan, V., Moeller, J., Mentis, M., Nakamura, T., Antonini, A., Eidelberg, D., 2000. Patterns of regional brain activation associated with different forms of motor learning. *Brain Res.* 871, 127–145.
- Inoue, K., Kawashima, R., Satoh, K., Kinomura, S., Sugiura, M., Goto, R., Ito, M., Fukuda, H., 2000. A pet study of visuomotor learning under optical rotation. *NeuroImage* 11, 505–516.
- Iramina, K., Ueno, S., Matsuoka, S., 1996. MEG and EEG topography of frontal midline theta rhythm and source localization. *Brain Topogr.* 8, 329–331.
- Jung, T.P., Makeig, S., Humphries, C., Lee, T.W., McKeown, M.J., Iragui, V., Sejnowski, T.J., 2000. Removing electroencephalographic artifacts by blind source separation. *Psychophysiology* 37, 163–178.
- Jung, T.P., Makeig, S., Westerfield, M., Townsend, J., Courchesne, E., Sejnowski, T.J., 2001. Analysis and visualization of single-trial event-related potentials. *Hum. Brain Mapp.* 14, 166–185.
- Kagerer, F.A., Contreras-Vidal, J.L., 1997. Adaptation as compared to sudden visuo-motor distortions. *Exp. Brain Res.* 115, 557–561.
- Kawashima, R., Roland, P.E., O'Sullivan, B.T., 1995. Functional anatomy of reaching and visuomotor learning: a positron emission tomography study. *Cereb. Cortex* 5, 111–122.
- Krakauer, J.W., Pine, Z.M., Ghilardi, M.F., Ghez, C., 2000. Learning of visuomotor transformations for vectorial planning of reaching trajectories. *J. Neurosci.* 20, 8916–8924.
- Lacquaniti, F., Perani, D., Guigon, E., Bettinardi, V., Carrozzo, M., Grassi, F., Rossetti, Y., Fazio, F., 1997. Visuomotor transformations for reaching to memorized targets: a PET study. *NeuroImage* 5, 129–146.
- Makeig, S., Westerfield, M., Jung, T.-P., Enghoff, S., Townsend, J., Courchesne, E., Sejnowski, T.J., 2002. Dynamic brain sources of visual evoked responses. *Science* 295, 690–694.
- Pfurtscheller, G., Stancak Jr., A., Edlinger, G., 1997. On the existence of different types of beta rhythms below 30 Hz. *Electroencephalogr. Clin. Neurophysiol.* 102, 316–325.
- Rodríguez-Fornells, A., Kurzbuch, A.R., Münte, T.F., 2002. Time course of error detection and correction in humans: neurophysiological evidence. *J. Neurosci.* 22, 9990–9996.
- Roby-Brami, A., Burnod, Y., 1995. Learning a new visuomotor transformation: error correction and generalization. *Brain Res. Cogn. Brain Res.* 2, 229–242.
- Seitz, R.J., Canavan, A.G., Yaguez, L., Herzog, H., Tellmann, L., Knorr, U., Huang, Y., Homberg, V., 1997. Representations of graphomotor trajectories in the human parietal cortex: evidence for controlled processing and automatic performance. *Eur. J. Neurosci.* 9, 378–389.
- Swick, D., Turken, A.U., 2002. Dissociating between conflict detection and error monitoring in the human anterior cingulate cortex. *PNAS* 99, 16354–16359.
- Vigario, R., Sarela, J., Jousmaki, V., Hamalainen, M., Oja, E., 2000. Independent component approach to the analysis of EEG and MEG recordings. *IEEE Trans. Biomed. Eng.* 47, 589–593.
- von Stein, A., Sarnthein, J., 2000. Different frequencies for different scales of cortical integration: from local gamma to long range alpha/theta synchronization. *Int. J. Psychophysiol.* 138, 301–313.
- Wolpert, D.M., Goodbody, S.J., Husain, M., 1998. Maintaining internal representations: the role of the human superior parietal lobe. *Nat. Neurosci.* 1, 529–533.